Journal of Magnetism and Magnetic Materials 511 (2020) 166995

Contents lists available at ScienceDirect

Journal of Magnetism and Magnetic Materials

journal homepage: www.elsevier.com/locate/jmmm

Research articles

Voltage-induced inertial domain wall motion in an antiferromagnetic nanowire

Fa Chen, Zhendong Zhang[1], Wei Luo*, Xiaofei Yang, Long You, Yue Zhang*

School of Optical and Electronic Information, Huazhong University of Science and Technology, Wuhan, 430074, PR China

ABSTRACT

In this article, we report our theoretical investigation about antiferromagnetic (AFM) DW motion induced by a gradient of magnetic anisotropy energy under a voltage pulse. The dynamics equation for the DW motion was derived. The solution indicates that the DW velocity is higher than 100 m/s, and because of inertia, the DW can keep moving at a speed of around 100 m/s for several nanoseconds after turning off the voltage in a period of the pulse. The mechanism for this DW inertia is explained based on the Lagrangian route. On the other hand, a spin wave is emitted while the DW is moving, yet the DW is still able to move at an increasing velocity with enlarging DW width. This indicates energy loss from the emission of spin-wave is less than the energy gain from the effective field of the gradient of anisotropy energy.

Novel racetrack magnetic memory devices with small volume and high reading speed is based on the motion of magnetic domain walls (DWs) in nanowires [1]. In general, the DW motion that arises from magnetization rotation can be triggered by either a magnetic field or a spin-polarized electrical current (or spin current) that is generated from an injected electrical current [1–12]. However, high dissipation from the injected electrical current is still a bottleneck for the application of a racetrack memory device. In recent years, more and more attention has been paid on researches about DW motion triggered by other forces with lower dissipation, such as voltage/electrical field [13–16], spin-wave [17,18], and acoustic wave [19,20]. In voltage-induced-DW-motion (VIDWM), a magnetic nanowire is deposited on a wedge-shaped insulating medium, and an external voltage generates a gradient of magnetic anisotropy energy that leads to spontaneous DW motion towards the edge of nanowire with a lower magnetic anisotropy energy [21,22] (Fig. 1).

In the past, researches were concentrated on DW motion in a ferromagnetic (FM) nanowire. In recent years, special dynamical behaviors of magnetic textures in other sorts of magnetic materials, such as antiferromagnet (AFM) [23–28], synthetic antiferromagnet (SAF) [29–31], ferrimagnet [32–36], and magnetic frustrate [37–40], have been revealed. Typical examples in these cases include ultra-high velocity and depressed Walker breakdown for coupled DWs in an SAF [29,30], relativistic-like width contraction for an AFM DW, and AFM DW-magneton interaction [23–25,27]. In an AFM, the DW moves at a high velocity with a weak stray field, which is vital to the racetrack memory device with a high reading speed and a small volume.

Very recently, electrical manipulation of AFM properties has attracted attention. For example, Néel vector in an AFM material can be induced to rotate under an electric field [41,42]. Wen et al have reported their theoretical analysis about VIDWM in an AFM system based on the assumption of DW motion at a *constant* velocity [43]. However, real DW motion is usually more complicated than simple uniform linear motion. Factually, DW motion is analogous to the motion of an object with mass, and physical quantities, such as mass, momentum, and inertia, are usually exploited to analyze DW motion in theory. For example, an effective mass is proposed based on the variation of kinetic energy of a DW driven by a magnetic field [44]. In current-induced DW motion, DW inertia due to transfer of momentum from propagating electrons to DW has been predicted theoretically and confirmed experimentally [45–47]. Similarly, AFM DW also exhibits inertia because of the secondary differential term in the dynamics equation for depicting DW motion [23,24]. Because of inertia, AFM DW motion should be more complicated than uniform linear motion, especially for DW motion induced by a short pulse that is commonly used in application.

In this article, we report our theoretic calculation about inertial DW motion at a high velocity (around 100 m/s) in an AFM nanowire driven by a gradient of magnetic anisotropy energy induced by a constant or pulsed voltage (Fig. 1). The AFM nanowire is deposited on a wedge-shaped insulating layer with thickness decreasing from left to right. Under a voltage applied between the top and bottom surface of the insulating layer, an electric field is generated in the insulating layer and enhances gradually from left to right. Because of electric-field control of magnetic anisotropy energy, a spatial dependent magnetic anisotropy

* Corresponding authors.
E-mail addresses: hustluowei@gmail.com (W. Luo), yue-zhang@hust.edu.cn (Y. Zhang).
[1] The author who has the same contribution with Fa Chen.

https://doi.org/10.1016/j.jmmm.2020.166995
Received 25 March 2020; Received in revised form 30 April 2020; Accepted 11 May 2020
Available online 19 May 2020
0304-8853/

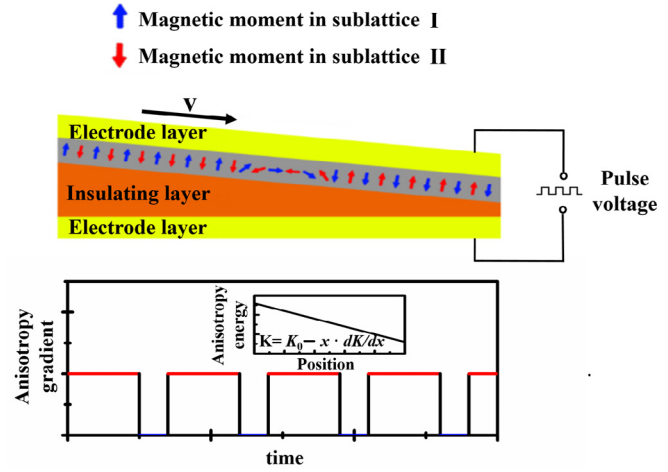

Fig. 1. Schematic of the principle of the pulsed voltage induced DW motion in an AFM system: AFM DW is induced to move under a pulsed voltage that generates a spatially dependent magnetic anisotropy energy with a pulsed gradient of anisotropy constant.

constant is generated in the AFM nanowire. For simplicity, we assume the anisotropy constant decreases linearly from left to right. The dynamics equation depicting the VIDWM is firstly derived from the Landau-Liftshiz-Gilbert (LLG) equation based on the model of an AFM nanowire with two FM sublattices (I and II) (Fig. 1). The AFM magnetic moments are distributed in a 3D medium but we only consider AFM exchange coupling along the length direction of the nanowire. The magnetization in the sublattice I (II) is expressed as $\vec{M}_{I(II)} = M_S\vec{m}_{I(II)}$, and M_S is the saturation magnetization of each sublattice, and $\vec{m}_{I(II)}$ is the unit vector for the orientation of magnetization.

The Hamiltonian of this AFM model is [23]:

$$H_{1D} = \frac{L_y L_z}{\Delta_j \Delta_k}[J \sum_{\langle I,II\rangle}^{N,N} \vec{m}_I \cdot \vec{m}_{II} - K_z(\sum_{I}^{N} m_{Iz}^2 + \sum_{II}^{N} m_{IIz}^2)] \tag{1}$$

In Eq. (1), J is the exchange constant for the nearest AFM exchange coupling. K_z is the uniaxial anisotropy constant. L_y, L_z, Δ_j, and Δ_k are the width, thickness, and cell size in the width and thickness direction, respectively. The uniform magnetization and staggered order parameters for the ith cell $\vec{m}_i$ and $\vec{n}_i$ are introduced as:

$$\vec{m}_i = (\vec{m}_I)_i + (\vec{m}_{II})_i \tag{2}$$

$$\vec{n}_i = [(\vec{M}_I)_i - (\vec{M}_{II})_i]/l \tag{3}$$

Here l is the absolute value of $(\vec{M}_I)_i - (\vec{M}_{II})_i$and close to $2M_S$ for strong exchange coupling.

Under continuum approximation and neglecting edge magnetization and parity-breaking term [23], Eq. (3) is converted into:

$$H_{1D} \approx \int_v \left(\frac{a}{2}m^2 + \frac{A}{2}\left(\frac{d\vec{n}}{dx}\right)^2 - Kn_z^2\right)d\tau \tag{4}$$

In Eq. (4), a is a homogeneous exchange energy ($a = 5\ J/V_{cell}$); A is an exchange stiffness constant ($A = J\Delta_i{}^2/V_{cell}$) and $K = K_z/V_{cell}$. Here Δ_i and V_{cell} represent cell size in the length direction and the volume of AFM unit cell, respectively.

Based on Eq. (4), the effective magnetic fields for$\vec{m}$and $\vec{n}$ were derived using the calculus of variations [24]:

$$\vec{H}_m = -\frac{\delta H_{1D}}{\mu_0 \delta \vec{m}} = -\frac{a\vec{m}}{\mu_0} \tag{5}$$

and

$$\vec{H}_n = -\frac{\delta H_{1D}}{\mu_0 \delta \vec{n}} = \frac{1}{\mu_0}\left(A\frac{d^2\vec{n}}{dx^2} + 2Kn_z\vec{e}_z\right) \tag{6}$$

Here, μ_0 is the permittivity of vacuum.

Starting from the LLG equation, we have formulated the dynamics equations for $\vec{m}$and $\vec{n}$ under strong exchange coupling:

$$\partial_t\vec{m} = -\frac{\gamma}{M_S}\vec{n} \times \vec{H}_n + \frac{G_2}{M_S}\vec{n} \times \partial_t\vec{n} \tag{7}$$

$$\partial_t\vec{n} = -\frac{\gamma}{M_S}\vec{n} \times \vec{H}_m + G_1 M_S \vec{n} \times \partial_t\vec{m} \tag{8}$$

Here G_1 and G_2 are the effective damping parameters for $\vec{n}$ and $\vec{m}$ ($G_1 = \alpha/l$, and $G_2 = \alpha l$). Combing Eqs. (7) and (8) under linear approximation and considering $G_1 \ll G_2$, we have derived the dynamics equations for $\vec{n}$:

$$\dot{\vec{n}} + \frac{G_2}{fM_S}\dot{\vec{n}} = \frac{\gamma}{fM_S}\vec{H}_n \tag{9}$$

Here $f = \mu_0 M_S(1 + G_1G_2)/a\gamma$, and $\vec{n} = \vec{n}(x, \{q_1(t), q_2(t)\})$with q_1 and q_2 representing two collective coordinates of DW. Multiplying $\frac{\partial\vec{n}}{\partial q_1}$ and $\frac{\partial\vec{n}}{\partial q_2}$at the two sides of Eq. (9) and integrating them over the whole nanowire, one can get the following equation:

$$\overleftrightarrow{M}\cdot\ddot{\vec{q}} + \frac{G_2}{fM_S}\overleftrightarrow{M}\cdot\dot{\vec{q}} = \vec{F} \tag{10}$$

In Eq. (10), $\overleftrightarrow{M}$is the tensor of effective mass with its component $M_{ij} = \int_{-\infty}^{+\infty}\frac{\partial\vec{n}}{\partial q_i}\cdot\frac{\partial\vec{n}}{\partial q_j}dx$, and $F_i = \frac{\gamma}{fM_S}\int_{-\infty}^{+\infty}\vec{H}_n\cdot\frac{\partial\vec{n}}{\partial q_i}dx$

In a Néel-type DW wall, $q_1 = q$, and $q_2 = \phi$, and$\vec{n} = (\sin\theta\cos\phi, \sin\theta\sin\phi, \cos\theta)$, in which $\theta = 2\arctan\{\exp[(x-q)/\lambda\}$with $\lambda = \sqrt{A/K}$for DW width [23,24]. Here $K = K_0 - (dK/dx)x$ [26], and we neglect the variation of DW width. Finally, the dynamics equation for q was derived:

$$\ddot{q} + \frac{G_2}{fM_S}\dot{q} = \frac{\gamma\lambda^2}{\mu_0 fM_S}\frac{dK}{dx} \tag{11}$$

Eq. (11) is solved based on the parameters of NiO [24,48]: K_0, M_S, d, γ, and μ_0 are 3.32×10^5 J/m^3, 4.25×10^5 A/m, 4.2×10^{-10} m, 2.21×10^5 m/A·s, and $4\pi \times 10^{-7}$N/A^2, respectively. Here M_S is estimated from the magnetic moment per sublattice ($1.7\mu_B$ with μ_B representing the Bohr magneton) A, α, and dK/dx are in the range of 3×10^{-13} J/m ~ 9×10^{-13} J/m, 1×10^{-4}~8×10^{-4}, and 0 GJ/m^4 ~300 GJ/m^4.

VIDWM has also been investigated numerically using the micromagnetic simulation software Object-Oriented Micromagnetic Framework (OOMMF). The track dimension is 3000 nm (length) × 1 nm (width) × 0.5 nm (thickness), and the cell dimension is 0.5 nm × 0.5 nm × 0.5 nm. Since OOMMF does not contain the code for the physical properties of an AFM sublattice, the parameters for above theoretical calculation cannot be directly used in the simulation, and modification is necessary. As magnetic moments with an AFM order are aligned in x direction in the theoretical analysis (a quasi-1D model), the unit cell for an AFM *sublattice* is twice as big as that for a single magnetic moment in OOMMF. Therefore, the M_S in OOMMF doubles with respect to that in the theoretical analysis. On the other hand, the exchange stiffness constant A in the theoretical analysis is also modified by considering a small difference between the lattice constant in theory and the cell size in OOMMF. The A for theoretical analysis (A_t) and that for simulation (A_s) satisfy the relationship $A_t = (d/a)A_s$. Here d and a are the cell size in the simulation (0.5 nm) and the lattice constant in theory (0.42 nm), respectively. Based on the above parameter modification, the simulated DW structure in the initial stable state is very close to the theoretical ansatz (Fig. 2(a)).

Initially, Eq. (11) is solved under the parameters dK/dx = 200 GJ/

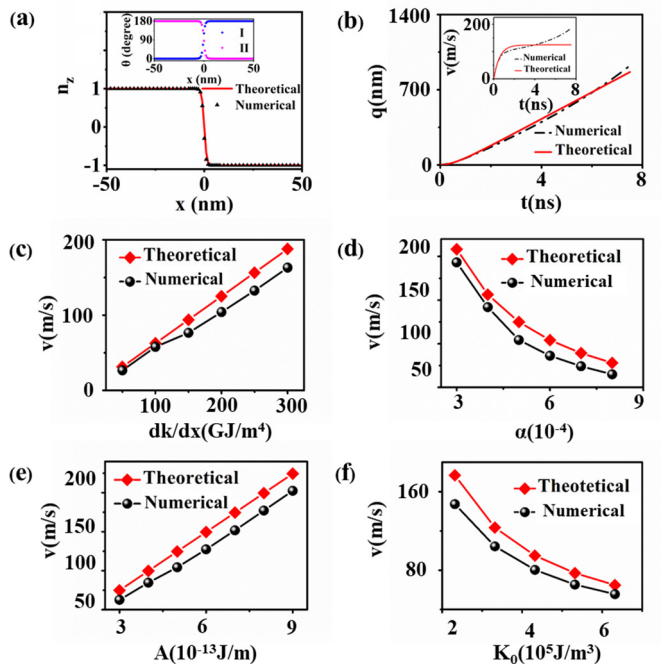

Fig. 2. (a). Néel vector across the region of DW in the initial state (The red solid line and black point show the theoretical ansatz and numerical data, respectively. The inset shows the simulated polar angles of the magnetic moments in two sublattices.) (b). Temporal displacement of AFM DW under a 200-GJ/m^4 dK/dx (Inset: Temporal DW velocity); (c)–(f). Theoretical stable DW velocity (red) and the DW velocity in the turning point of the simulated velocity/time curves (black) as a function of dK/dx, damping coefficient α, exchange stiffness constant A, and the intercept K_0 in the x dependence of K. (For interpretation of the references to colour in this figure legend, the reader is referred to the web version of this article.)

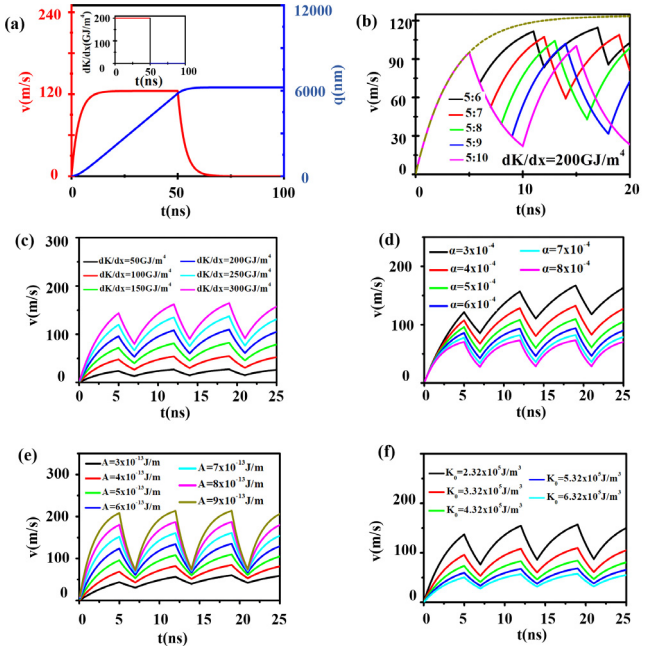

Fig. 3. (a). Temporal displacement and velocity of AFM DW under the gradient of magnetic anisotropy constant dK/dx as indicated in the inset, (b). Temporal velocity of AFM DW under a 200-GJ/m^4 pulsed dK/dx with different duty ratios (The dashed line indicates the temporal DW velocity under the constant dK/dx of 200 GJ/m^4), (c)~(f). Temporal velocity of AFM DW driven by the gradient of magnetic anisotropy energy as a function of (c) exchange stiffness constant A, (d) intercept of the x dependent K (K_0), (e) gradient of magnetic anisotropy constant dK/dx, and (f) damping coefficient α.

m^4, $\alpha = 5 \times 10^{-4}$, and $A = 5 \times 10^{-13}$ J/m. The result (red solid line in Fig. 2(b)) indicates that DW moves at an increasing velocity in the initial 2 ns, and the velocity reaches a stable value (around 120 m/s). The magnitude of DW velocity is the same as that of voltage-induced skyrmion motion [26]. The result of numerical simulation (the black dashed line) is very close to the solution of Eq. (11) in the first 4 ns. Afterwards, the simulated DW motion becomes faster. This acceleration arises from the increase of DW width that is neglected in the theoretical calculation.

Based on the theoretical analysis and numerical simulation, the influence of dK/dx, α, and A on DW velocity was studied in detail. When dK/dx increases from 0 to 300 GJ/m^4, the stable DW velocity in theory increases monotonously to around 200 m/s (α and A are 5×10^{-4} and 5×10^{-13} J/m, respectively.). When α increases from 1×10^{-4} to 8×10^{-4}, the DW velocity decreases from around 200 m/s to about 80 m/s (dK/dx and A are 200 GJ/m^4 and $A = 5 \times 10^{-13}$ J/m, respectively.) (Fig. 2(d)). This indicates low damping is favorable for fast DW motion. Such a low α of around 10^{-4} has been observed in NiO experimentally [48]. On the other hand, the increase of A from 5×10^{-13} J/m to 9×10^{-13} J/m enhances the DW velocity from 75 m/s to about 230 m/s (α and dK/dx are fixed at 5×10^{-4} and 200 GJ/m^4.) (Fig. 2(e)). Additionally, the increase of the intercept K_0 in $K(x)$ reduces the DW velocity (Fig. 2(f)). The DW velocity in the turning point of the simulated velocity/time curve was compared with the stable velocity in theory. The results of simulation are close to that of theoretical calculation, and the difference between them is small when dK/dx is small or K_0 is high. In either case, the relative variation of DW width in the process of DW motion is small.

Owing to the second differential of q with respect to time, AFM DW motion exhibits inertia, i.e., DW experiences an acceleration/deceleration stage after the voltage is turned on/off. To investigate this inertial DW motion, the constant dK/dx was replaced by a pulsed dK/dx. As a representative example for DW motion driven by a single pulse (dK/dx = 200 GJ/m^4) with a duration of 50 ns, a gradual acceleration and deceleration for around 20 ns appears soon after the pulse is turned on and off (Fig. 3(a)). As to the current-induced DW motion in an FM nanowire, the secondary differential equation of central position can be also derived by deleting the azimuthal angle in the equation group of collective coordinates [49]. However, since the central position is strictly coherent to the azimuthal angle, the effective mass of an FM DW still changes with variation of DW structure in the process of DW motion [49]. In contrast, in the VIDWM in an AFM nanowire, the diagonal components of effective mass tensor include $M_{11} = 2/\lambda$ for q and $M_{22} = 2\lambda$ for ϕ, and both cross-terms M_{12} and M_{21} are zero. This means that q is independent of ϕ, and the effective mass keeps constant in the process of DW motion.

The inertia of AFM DW motion is influenced by the duty ratio of a pulsed dK/dx, A, α, K_0, and dK/dx (Fig. 3(b)–(f)). The temporal velocity of DW motion under a pulsed dK/dx with the duty ratio between 5:5 (constant dK/dx = 200 GJ/m^4) and 5:10 (5 ns for dK/dx = 200 GJ/m^4 and 5 ns for dK/dx = 0 GJ/m^4) shows that the DW keeps moving at an average velocity of around 50 m/s when the zero-dK/dx stage lasts 5 ns (Fig. 3(b)). On the other hand, with enhancing A, decreasing K_0, or increasing dK/dx, the DW motion under a non-zero dK/dx and the decaying of DW velocity in the zero-dK/dx stage become faster (Fig. 3(c)–(f)). Reducing α enhances the DW velocity under a non-zero dK/dx but also slows down the decaying of DW velocity under a zero dK/dx. Therefore, a low damping coefficient is important for the DW motion at a *sustainable* high velocity.

The mechanism of inertia can be understood using the Lagrangian approach. The Lagrangian density Ω equals $T - V$ with T and V representing kinetic and free energy density, respectively. V is the integrand in Eq. (4), while T is [23]:

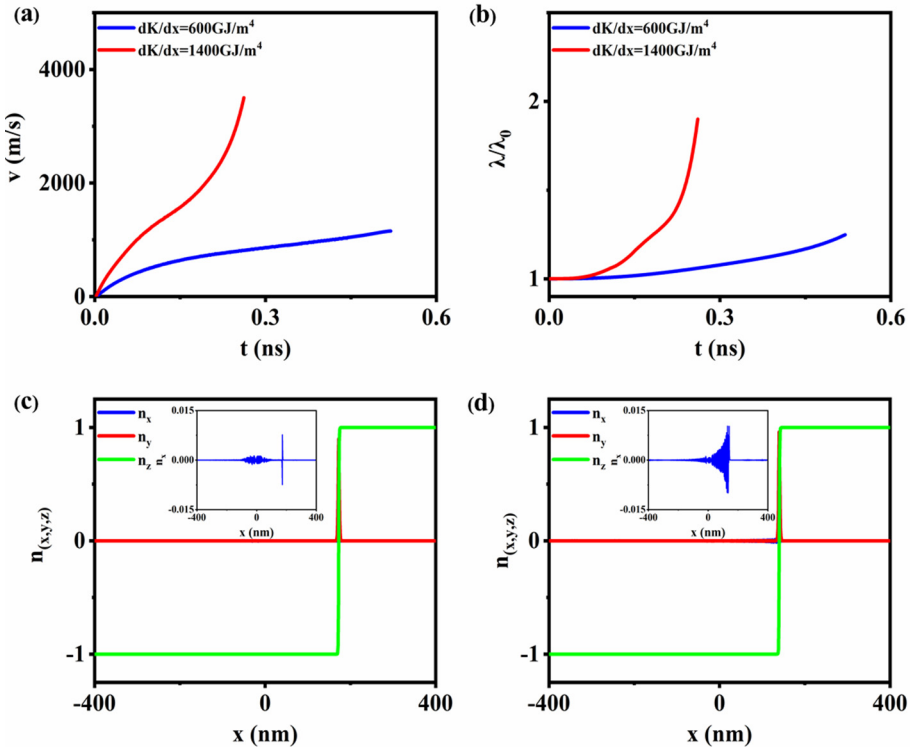

Fig. 4. (a) Temporal DW velocity under two different dK/dx; (b). evolution of DW width relative to that for a static one under two different dK/dx; (c). x, y, z components of Néel vector for a moving DW under 600-GJ/m^4 dK/dx at a velocity of around 800 m/s; (d). x, y, z components of Néel vector for a moving DW under 1400-GJ/m^4 dK/dx at a velocity of around 1500 m/s.

$$T = \rho\vec{m}\cdot(\dot{\vec{n}} \times \vec{n}) \tag{12}$$

Here, ρ is a constant that is proportional to spin angular momentum [23]. For an AFM system with a nonzero damping coefficient, a dissipation density function R is introduced as [50]:

$$R = \tilde{\alpha}(\dot{\vec{n}})^2 \tag{13}$$

Here $\tilde{\alpha}$ is a phenomenological factor. The Lagrangian (L) and Rayleigh dissipation function F were derived via integrating T and R throughout the AFM nanowire, and they satisfy the Lagrange-Rayleigh equation:

$$\frac{d}{dt}\left(\frac{\partial L}{\partial \dot{q}}\right) = \frac{\partial L}{\partial q} + \frac{\partial F}{\partial \dot{q}} \tag{14}$$

Here $\frac{\partial L}{\partial \dot{q}}$, $\frac{\partial L}{\partial q}$, and $\frac{\partial F}{\partial \dot{q}}$ are canonical momentum (P), canonical force, and dissipation force, respectively. Combining Eqs. (12) to (14), we have derived the dynamics equation of P:

$$\frac{dP}{dt} = -\frac{2\tilde{\alpha}}{f(2\rho - af)}P + N\frac{dK}{dx} \tag{15}$$

In Eq. (15), P and N are:

$$P = \frac{\partial L}{\partial \dot{q}} = 4L_yL_z\frac{f}{\lambda}\left(\rho - \frac{af}{2}\right)\dot{q} + L_yL_z\alpha\lambda\left(f - \frac{\rho}{a}\right)\frac{dK}{dx} \tag{16}$$

$$N = \frac{2L_yL_z\alpha\tilde{\alpha}\lambda}{f(2\rho - af)}\left(f - \frac{\rho}{a}\right) + L_yL_z\frac{2\alpha^2\lambda}{3a}\left(K_0 - \frac{dK}{dx}q\right) - L_yL_z\frac{\alpha^2 A}{3a\lambda} - L_yL_z C_1\lambda \tag{17}$$

Here, C_1 is an integral constant $C_1 = \int_{-\frac{L_x}{2}}^{\frac{L_x}{2}} \tanh^2\varepsilon d\varepsilon$.

Eqs. (16) shows that P is composed of two terms: one is similar to mechanical momentum, and the other one contributed from the gradient of anisotropy energy is analogous to the momentum of the magnetic field that induces motion of a charged particle. Under a non-zero dK/dx, the momentum evolves gradually towards a stable value based on Eq. (15). While after dK/dx retreats, P decays exponentially. This is consistent with the inertia of the DW motion described above.

In addition to inertia, the motion of AFM DW also usually experiences Lorentz contraction, i.e., DW width decreases when DW velocity increases towards a limit value that is determined by the group velocity of a spin wave (v_g) [25]. When DW velocity approaches v_g, DW energy is released by emitting a spin wave, which inhibits further increase in DW velocity. Similar spin-wave emission has also been observed in electric-field driven FM DW motion but the mechanism is different [16].

In the previous analysis, we did not consider the variation of DW width. This is reasonable under a moderate dK/dx. When the DW is driven under a high dK/dx, the variation of DW width is not negligible. In theory, DW motion with acceleration is expected if the variation of DW width is also considered [21]. Using micromagnetic simulation, we have compared the temporal DW velocity and DW width under different dK/dx (Fig. 4(a) and (b)). When dK/dx = 600 GJ/m^4, both DW velocity and DW width increase slowly. Nevertheless, when dK/dx = 1400 GJ/m^4, DW velocity increases drastically with a turning point appearing in the DW velocity ~ time curve, which is accompanied with obvious widening of DW. On the other hand, it is noticed that a spin wave is also emitted when the DW moves at a high velocity (Fig. 4(c) and (d)). However, this emission of spin wave does not inhibit the enhancing of DW velocity. On the contrary, the amplitude of the spin wave increases with increasing DW velocity. Since a gradient of anisotropy energy can be converted into an effective magnetic field that becomes stronger with decreasing anisotropy constant [21], a sustainable increase in DW velocity indicates the energy gain from this enhancing effective field exceeds the energy loss from the emission of a spin wave.

In summary, we have derived the dynamics equation for describing DW motion in an AFM nanowire under a moderate gradient of magnetic anisotropy energy. The solution indicates the DW velocity is enhanced by enhancing the exchange stiffness constant, reducing the damping coefficient, or increasing the slope or reducing the intercept of the anisotropy energy that varies linearly with the spatial coordinate. Because of inertia, the DW is able to keep moving for several nanoseconds after retreating the gradient of magnetic anisotropy energy,

and a low damping coefficient is vital to the DW motion at a sustainable high velocity. This DW inertia can be interpreted from the dynamics of canonical momentum that is derived from the Lagrangian approach. On the other hand, even though a spin wave is emitted, the DW velocity still keeps increasing under a high gradient of anisotropy energy, showing that the gradient of anisotropy energy offers more energy than the energy loss from the emission of spin wave.

CRediT authorship contribution statement

Fa Chen: Data curation, Formal analysis, Writing-original draft, Software. **Zhendong Zhang:** Data curation, Formal analysis, Software. **Wei Luo:** Methodology, Supervision, Writing-review and editing. **Xiaofei Yang:** Methodology, Supervision. **Long You:** Methodology, Supervision. **Yue Zhang:** Conceptualization, Methodology, Supervision, Writing-review and editing, Funding acquisition.

Declaration of Competing Interest

The authors declare that they have no known competing financial interests or personal relationships that could have appeared to influence the work reported in this paper.

Acknowledgments

The authors acknowledge financial support from the National Natural Science Foundation of China (No. 51971098) and Science and Technology Department of Hubei Province (No. 2019CFB435).

Appendix A. Supplementary data

Supplementary data to this article can be found online at https://doi.org/10.1016/j.jmmm.2020.166995.

References

[1] S.S.P. Parkin, M. Hayashi, L. Thomas, Magnetic domain-wall racetrack memory, Science 320 (2008) 190–194.
[2] G.S.S. Beach, C. Nistor, C. Knutson, M. Tsoi, J.L. Erskine, Dynamics of field-driven domain-wall propagation in ferromagnetic nanowires, Nat. Mater. 4 (10) (2005) 741–744.
[3] M.A. Bahri, B. Borie, T.L. Jin, R. Sbiaa, M. Kläui, S.N. Piramanayagam, Staggered magnetic nanowire devices for effective domain-wall pinning in racetrack memory, Phys. Rev. Appl. 11 (2019) 024023.
[4] M. Hayashi, L. Thomas, R. Moriya, C. Rettner, S.S.P. Parkin, Current-controlled magnetic domain-wall nanowire shift register, Science 320 (2008) 209–211.
[5] A. Brataas, A.D. Kent, H. Ohno, Current-induced torques in magnetic materials, Nat. Mater. 11 (2012) 372–381.
[6] I.M. Miron, T. Moore, H. Szambolics, L.D. Buda-Prejbeanu, S. Auffret, B. Rodmacq, S. Pizzini, J. Vogel, M. Bonfim, A. Schuhl, Fast current-induced domain-wall motion controlled by the Rashba effect, Nat. Mater. 10 (2011) 419–423.
[7] A. Thiaville, Y. Nakatani, J. Miltat, Y. Suzuki, Micromagnetic understanding of current-driven domain wall motion in patterned nanowires, Europhys. Lett. 69 (2005) 990–996.
[8] P.P.J. Haazen, E. Murè, J.H. Franken, R. Lavrijsen, H.J.M. Swagten, B. Koopmans, Domain wall depinning governed by thespin Hall effect, Nat. Mater. 12 (2013) 299–303.
[9] K.S. Ryu, L. Thomas, S.H. Yang, S. Parkin, Chiral spin torque at magnetic domain walls, Nat. Nanotechnol. 8 (2013) 527–533.
[10] S. Emori, U. Bauer, S.M. Ahn, E. Martinez, G.S.D. Beach, Current-driven dynamics of chiral ferromagnetic domain walls, Nat. Mater. 12 (2013) 611–616.
[11] S. Emori, E. Martinez, K.J. Lee, H.W. Lee, U. Bauer, S.M. Ahn, P. Agrawal, D.C. Bono, G.S.D. Beach, Spin hall torque magnetometry of dzyaloshinskii domain walls, Phys. Rev. B 90 (2013) 184427.
[12] Z.C. Luo, A. Hrabec, T.P. Dao, G. Sala, S. Finizio, J.X. Feng, S. Mayr, J. Raabe, P. Gambardella, L.J. Heyderman, Current-driven magnetic domain-wall logic, Nature 579 (2020) 214–218.
[13] A.J. Schellekens, A. van den Brink, J.H. Franken, H.J.M. Swagten, B. Koopmans, Electric-field control of domain wall motion in perpendicularly magnetized materials, Nat. Commun. 3 (2012) 847.
[14] W. Lin, N. Vernier, G. Agnus, K. Garcia, B. Ocker, W. Zhao, E.E. Fullerton, D. Ravelosona, Universal domain wall dynamics under electric field in Ta/CoFeB/MgO devices with perpendicular anisotropy, Nat. Commun. 7 (2016) 13532.
[15] D. Chiba, M. Kawaguchi, S. Fukami, N. Ishiwata, K. Shimamura, K. Kobayashi, T. Ono, Electric-field control of magnetic domain-wall velocity in ultrathin cobalt with perpendicular magnetization, Nat. Commun. 3 (2012) 888.
[16] B.V.D. Wiele, L. Laurson, K.J.A. Franke, S.V. Dijken, Electric field driven magnetic domain wall motion in ferromagnetic-ferroelectric heterostructures, Appl. Phys. Lett. 104 (2014) 012401.
[17] X. Wang, G. Guo, Y. Nie, G. Zhang, Z. Li, Domain wall motion induced by the magnonic spin current, Phys. Rev. B 86 (2012) 054445.
[18] W. Wang, M. Albert, M. Beg, M. Bisotti, D. Chernyshenko, D. Cortés-Ortuño, I. Hawke, H. Fangohr, Magnon-driven domain-wall motion with the Dzyaloshinskii-Moriya interaction, Phys. Rev. Lett. 114 (2015) 087203.
[19] J. Dean, M.T. Bryan, J.D. Cooper, A. Virbule, J.E. Cunningham, T.J. Hayward, A sound idea: Manipulating domain walls in magnetic nanowires using surface acoustic waves, Appl. Phys. Lett. 107 (2015) 142405.
[20] W. Edrington, U. Singh, M.A. Dominguez, J.R. Alexander, R. Nepal, S. Adenwalla, SAW assisted domain wall motion in Co/Pt multilayers, Appl. Phys. Lett. 112 (2018) 052402.
[21] Y. Zhang, S. Luo, X. Yang, C. Yang, Spin-orbit-torque-induced magnetic domain wall motion in Ta/CoFe nanowires with sloped perpendicular magnetic anisotropy, Sci. Rep. 7 (2017) 2047.
[22] K. Yamada, S. Murayama, Y. Nakatani, Magnetic domain wall motion in Co/Ni nanowires induced by a sloped electric field, Appl. Phys. Lett. 108 (2016) 202405.
[23] E.G. Tveten, T. Müller, J. Linder, A. Brataas, Intrinsic magnetization of antiferromagnetic textures, Phys. Rev. B 93 (2019) 104408.
[24] E.G. Tveten, A. Qaiumzadeh, A. Brataas, Antiferromagnetic domain wall motion induced by spin waves, Phys. Rev. Lett. 112 (2014) 147204.
[25] T. Shiino, S.H. Oh, P.M. Haney, S.W. Lee, G. Go, B.G. Park, K.J. Lee, Antiferromagnetic domain wall motion driven by spin-orbit torques, Phys. Rev. Lett. 117 (2016) 087203.
[26] L. Shen, J. Xia, G. Zhao, X. Zhang, M. Ezawa, O.A. Tretiakov, X. Liu, Y. Zhou, Dynamics of the antiferromagnetic skyrmion induced by a magnetic anisotropy gradient, Phys. Rev. B 98 (2018) 134448.
[27] E.G. Tveten, A. Qaiumzadeh, O.A. Tretiakov, A. Brataas, Staggered dynamics in antiferromagnets by collective coordinates, Phys. Rev. Lett. 110 (2013) 127208.
[28] L. Sánchez-Tejerina, V. Puliafito, P.K. Amiri, M. Carpentieri, G. Finocchio, Dynamics of domain-wall motion driven by spin-orbit torque in antiferromagnets, Phys. Rev. B 101 (2020) 014433.
[29] S. Yang, K. Ryu, S. Parkin, Domain-wall velocities of up to 750 m s^{-1} driven by exchange-coupling torque in synthetic antiferromagnets, Nat. Nanotechnol. 10 (2015) 221–226.
[30] L. Chen, M. Shen, Y. Peng, X. Liu, W. Luo, X. Yang, L. You, Y. Zhang, Voltage-induced high-speed DW motion in a synthetic antiferromagnet, J. Phys. D Appl. Phys. 52 (2019) 495001.
[31] C. Ma, X. Zhang, J. Xia, M. Ezawa, W. Jiang, T. Ono, S.N. Piramanayagam, A. Morisako, Y. Zhou, X. Liu, Electric field-induced creation and directional motion of domain walls and skyrmion bubbles, Nano Lett. 19 (2019) 353–361.
[32] S. Oh, S.K. Kim, J. Xiao, K. Lee, Bidirectional spin-wave-driven domain wall motion in ferrimagnets, Phys. Rev. B 100 (2019) 174403.
[33] E. Haltz, J. Sampaio, R. Weil, Y. Dumont, A. Mougin, Strong current actions on ferrimagnetic domain walls in the creep regime, Phys. Rev. B 99 (2019) 104413.
[34] E. Martínez, V. Raposo, Ó. Alejos, Current-driven domain wall dynamics in ferrimagnets: Micromagnetic approach and collective coordinates model, J. Magn. Magn. Mater. 491 (2019) 165545.
[35] Y. Hirata, D.H. Kim, S.K. Kim, D.K. Lee, S.H. Oh, D.Y. Kim, T. Nishimura, T. Okuno, Y. Futakawa, H. Yoshikawa, A. Tsukamoto, Y. Tserkovnyak, Y. Shiota, T. Moriyama, S.B. Choe, K.J. Lee, T. Ono, Vanishing skyrmion Hall effect at the angular momentum compensation temperature of a ferrimagnet, Nat. Nanotechnol. 14 (2019) 232–236.
[36] W.H. Li, Z. Jin, D.L. Wen, X.M. Zhang, M.H. Qin, J.-M. Liu, Ultrafast domain wall motion in ferrimagnets induced by magnetic anisotropy gradient, Phys. Rev. B 101 (2020) 024414.
[37] T. Kurumaji, T. Nakajima, M. Hirschberger, A. Kikkawa, Y. Yamasaki, H. Sagayama, H. Nakao, Y. Taguchi, T.H. Arima, Y. Tokura, Skyrmion lattice with a giant topological Hall effect in a frustrated triangular-lattice magnet, Science 365 (2019) 914–918.
[38] Kosuke Karube, Jonathan S. White, Daisuke Morikawa, Charles D. Dewhurst, Robert Cubitt, Akiko Kikkawa, Xiuzhen Yu, Yusuke Tokunaga, Taka-hisa Arima, Henrik M. Rønnow, Yoshinori Tokura, Yasujiro Taguchi, Disordered skyrmion phase stabilized by magnetic frustration in a chiral magnet, Sci. Adv. 4 (9) (2018) eaar7043, https://doi.org/10.1126/sciadv.aar7043.
[39] B. Heil, A. Rosch, J. Masell, Universality of annihilation barriers of large magnetic skyrmions in chiral and frustrated magnets, Phys. Rev. B 100 (2019) 134424.
[40] Z. Hou, Q. Zhang, X. Zhang, G. Xu, J. Xia, B. Ding, H. Li, S. Zhang, N.M. Batra, E. Pmfj Costa, G. Liu, M. Wu, X. Ezawa, Y. Liu, X. Zhang Zhou, W. Wang, Current-induced helicity reversal of a single skyrmionic bubble chain in a nanostructured frustrated magnet, Adv. Mater. 31 (2019) 1904815.
[41] I.J. Park, T. Lee, P. Das, B. Debnath, G.P. Carman, R.K. Lake, Strain control of the Neel vector in Mn-based antiferromagnets, Appl. Phys. Lett. 114 (2019) 142403.
[42] Z. Liu, Z. Feng, H. Yan, X. Wang, X. Zhou, P. Qin, H. Guo, R. Yu, C. Jiang, Antiferromagnetic piezospintronics, Adv. Electron. Mater. 5 (2019) 1900176.
[43] D.L. Wen, Z.Y. Chen, W.H. Li, M.H. Qin, D.Y. Chen, Z. Fan, M. Zeng, X.B. Lu, X.S. Gao, J.M. Liu, Intrinsic and extrinsic antiferromagnetic damping in NiO, Phys. Rev. Res. 2 (2020) 013166.
[44] G.T. Rado, On the inertia of oscillating ferromagnetic domain walls, Phys. Rev. 83 (1951) 821–826.
[45] S.E. Barnes, S. Maekawa, Current-spin coupling for ferromagnetic domain walls in fine wires, Phys. Rev. Lett. 95 (2005) 107204.

[46] L. Thomas, R. Moriya, C. Rettner, S.S.P. Parkin, Dynamics of magnetic domain walls under their own inertia, Science 330 (2010) 1810–1813.
[47] G. Tatara, H. Kohno, Theory of current-driven domain wall motion: spin transfer versus momentum transfer, Phys. Rev. Lett. 92 (2004) 086601.
[48] T. Moriyama, K. Hayashi, K. Yamada, M. Shima, Yutak Ohya, T. Ono, Intrinsic and extrinsic antiferromagnetic damping in NiO, Phys. Rev. Mater. 3 (2019) 051402 (R).
[49] J. Torrejon, E. Martinez, M. Hayashi, Tunable inertia of chiral magnetic domain walls, Nat. Commun. 7 (2016) 13533.
[50] R. Cheng, Q. Niu, Dynamics of antiferromagnets driven by spin current, Phys. Rev. B 89 (2014) 081105 (R).